AGU PUBLICATIONS

Geochemistry, Geophysics, Geosystems

RESEARCH ARTICLE
10.1002/2015GC005965

Oligocene-Miocene magnetostratigraphy and magnetic anisotropy of the Baxbulak section from the Pamir-Tian Shan convergence zone

Zihua Tang[1,2], Xinxin Dong[1], Xu Wang[1], and Zhongli Ding[1,2]

[1]Key Laboratory of Cenozoic Geology and Environment, Institute of Geology and Geophysics, Chinese Academy of Sciences, Beijing, China, [2]CAS Center for Excellence in Tibetan Plateau Earth Sciences, Beijing, China

Key Points:
- A terrestrial section from the Pamir-Tian Shan Convergence zone is magnetostatigraphically dated
- Magnetostratigraphic data assigns the sequence to the late Oligocene-early Miocene
- Magnetic fabric suggests an increased strain and regional counterclockwise rotation since 26 Ma

Supporting Information:
- Supporting Information S1

Correspondence to:
Z. Tang,
tangzihua@mail.iggcas.ac.cn;
tangzihua@yahoo.com

Citation:
Tang, Z., X. Dong, X. Wang, and Z. Ding (2015), Oligocene-Miocene magnetostratigraphy and magnetic anisotropy of the Baxbulak section from the Pamir-Tian Shan convergence zone, *Geochem. Geophys. Geosyst.*, *16*, 3575–3592, doi:10.1002/2015GC005965.

Received 17 JUN 2015
Accepted 29 SEP 2015
Accepted article online 5 OCT 2015
Published online 23 OCT 2015

Abstract As the northernmost part of the Indo-Eurasian collision belt, the Pamir-Tian Shan convergence zone (PTCZ) is a strategic location for understanding intracontinental deformation. Here we present a magnetostratigraphic investigation of a continuous section from the Baxbulak region, to better constrain regional tectonic history. Rock magnetic analyses indicate that hematite and magnetite are the main carriers of characteristic remanent magnetization. The resulting polarity sequence allows a distinct correlation to the geomagnetic polarity time scale, showing that the section spans the interval of 29.1–20.7 Ma. Rock magnetic results further suggest that paramagnetic and antiferromagnetic minerals dominantly contribute to anisotropy of magnetic susceptibility (AMS) of the sequence. Thus, the AMS would indicate the preferred orientations of the mineral grains that are sensitive to tectonic strain. At around 26 Ma, the grouped principal minimum perpendicular to the bedding diverts to a girdle distribution in a N-S direction, demonstrating the overprint of tectonic fabric to previous weakly deformed sedimentary fabric. This would be interpreted as a marked increase in tectonic strain, consistent with various evidence from the Pamir and the neighboring basin that show the Pamir began to migrate northward. Moreover, the coincident changes in distribution of AMS principal axes, in both direction and magnitude, are comparable to the regional counterclockwise rotations observed from paleomagnetic data, likely related to orogenesis.

1. Introduction

The Indo-Eurasian collision has caused extensive intercontinental deformation in Central Asia since the early Cenozoic. For example, the Pamir Plateau migrated northward by at least 600 km with respect to the stable Eurasia [*Burtman and Molnar*, 1993], creating an opportunity to study how the continental crust deforms. However, the plateau suffers from poorly dated terrestrial sediments and an absence of subduction-related volcanic units. Therefore, the timing and pattern of the tectonic evolution of the Pamir are still highly disputed.

On the flanks of the Pamir indentor, Cenozoic deformations are dominated by the sinistral Darvaz Fault bounding the Tajik Basin to the west and by the dextral Kashgar-Yecheng transfer system (KYTS) bounding the Tarim Basin to the east (Figure 1a). Paleomagnetic data from the Tajik Basin reveal systematic counterclockwise vertical-axis rotations [*Bazhenov and Burtman*, 1986; *Thomas et al.*, 1994; *Burtman*, 2000], which are generally attributed to northwest-directed radial thrusting of the Pamir [*Strecker et al.*, 1995]. In contrast to the west side, the timing and magnitude of rotations along the KYTS on the eastern flank seem to be site-dependent [e.g. *Chen et al.*, 1992; *Rumelhart et al.*, 1999; *Dupont-Nivet et al.*, 2002; *Huang et al.*, 2006a, 2009], even when an identical section is taken [e.g. *Li et al.*, 2013; *Bosboom et al.*, 2014a, 2014b]. Furthermore, a regional review of existing data leads to competing kinematic models for the Pamir indentation: radial thrusting inducing rotation on both sides [e.g., *Strecker et al.*, 1995], an asymmetric deformation, i.e., radial thrusting along the west margin and a dextral transfer system along the east margin [e.g., *Cowgill*, 2010], and a two stage "mixing" model, i.e., radial thrusting on the west prevailed throughout the Cenozoic, while the Paleogene radial thrusting was followed by Miocene transfer slip along the east side [e.g., *Bosboom et al.*, 2014a, 2014b]. These varied interpretations obscure the timing and approach of the building of the Pamir.

On the north of the Pamir indentor, the Tian Shan was reactivated during the Cenozoic as a result of the Indo-Asian collision [e.g., *Tapponnier and Molnar*, 1979; *Tang et al.*, 2012] with little or no northward

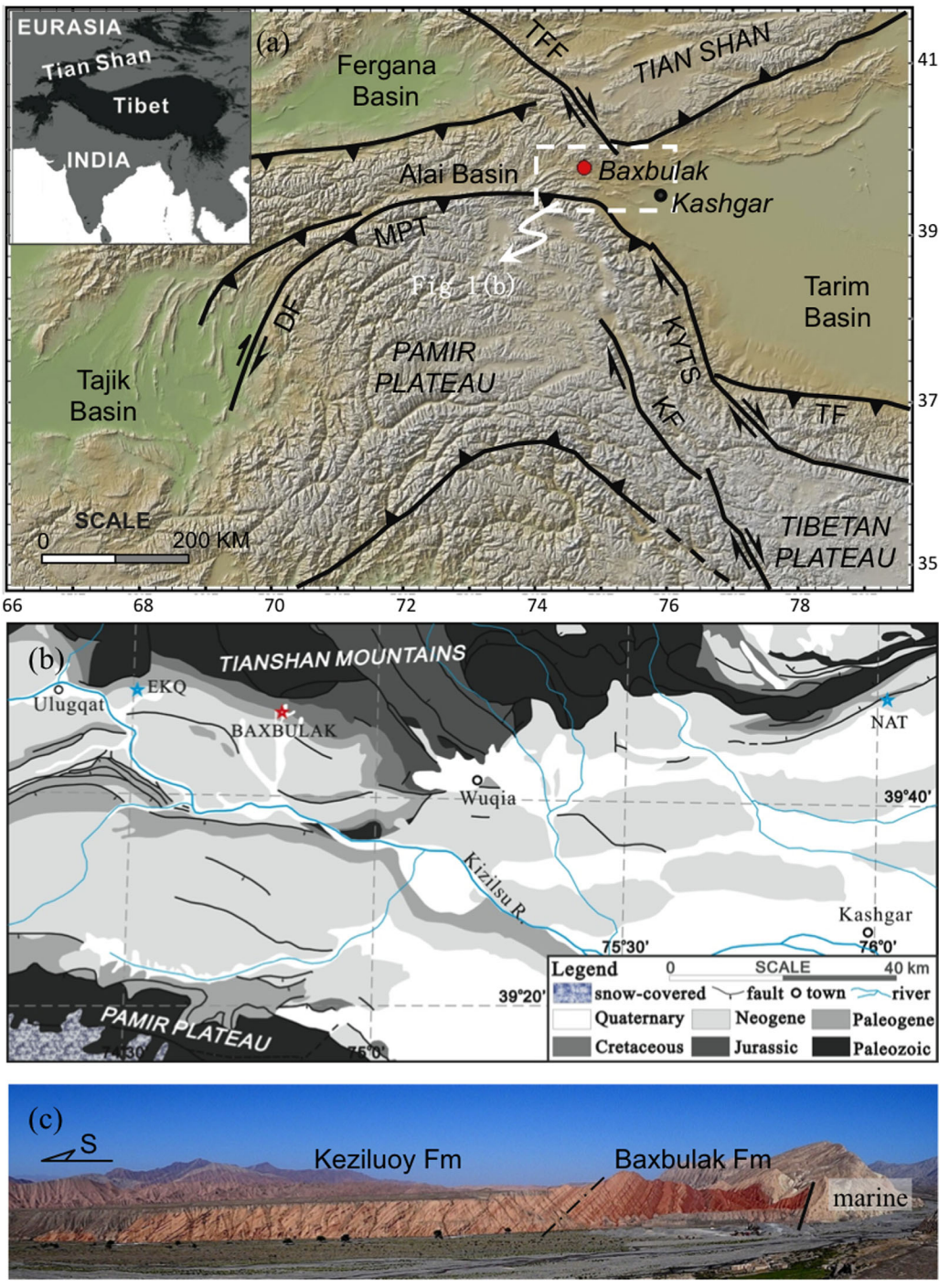

Figure 1. (a) Sketched relief map with major faults surrounding the Pamir, showing the location of the study section at the eastern part of the Pamir-Tian Shan convergence zone. Abbreviations: MPT – Main Pamir Thrust; TFF – Talas – Fergana Fault; DF – Darvaz Fault; KYTS – Kashgar-Yecheng transfer fault; KF – Karakoram Fault; TF – Tiklik Fault; (b) Simplified geological map of the study area with the other two sections, EKQ and NAT; and (c) Field photograph of the Baxbulak section.

convergence relative to Eurasia since ~60 Ma [*Huang et al*., 2006a]. South of the western Tian Shan is the Alai Basin, the last vestige of the Mesozoic to early Cenozoic sedimentary basin that formerly connected the Tajik and Tarim Basins [*Şengör*, 1984; *Burtman*, 2000]. On the south of the Basin, the Main Pamir Thrust (MPT) defines the leading edge of the Pamir Plateau. Correlation of the MPT and the Tiklik Fault (Figure 1a), at the northern and the southern end of the KYTS respectively, suggests ~300 km of total northward migration of the Pamir. Global Positioning System measurements also indicate that the present-day convergence

of 10–15 mm/a between the Pamir and the Alai Basin may be mainly absorbed by the MPT [*Reigber et al*., 2001; *Zubovich et al*., 2010]. As the most extensively deformed region, the convergence zone between the stationary Tian Shan and the indenting Pamir Plateau is a strategic place for recording regional tectonic evolution due to the Indo-Asian collision.

Cenozoic continental sediments in the Pamir-Tian Shan convergence zone (PTCZ, Figure 1b) record stratigraphic information and structural evolution during the orogeny. Here we use paleomagnetic observations to constrain the chronology and tectonics at the convergence between the Pamir Plateau and the Tian Shan. Additionally we present a record of anisotropy of magnetic susceptibility (AMS) for a clastic sedimentary outcrop from the eastern portion of the convergence zone, within detailed magnetostratigraphic framework, to discuss the timing of regional tectonic activities due to the Indo-Asian collision.

2. Geological Setting

Due to the consistent northward indentation of the Pamir Plateau, a formerly contiguous Tarim-Tajik Basin was gradually isolated during the Cenozoic. This convergent process not only forced the retreat of an epicontinental sea that once extended into the Tarim Basin [*Sun and Jiang*, 2013; *Bosboom et al*., 2011], but also formed a convergence zone between the Pamir and the Tian Shan, comprising an archive of history of intracontinental deformation [*Coutand et al*., 2002; *Burtman and Molnar*, 1993]. The stratigraphic succession consists of up to 1500 m of late Cretaceous-early Cenozoic shallow marine strata overlain by 3–10 km of continental clastic sediments, with increasing grain size and sedimentation rates up the section [*CGXSC*, 1981; *Coutand et al*., 2002].

In the eastern area of the PTCZ, as well as the eastern flank of the Pamir, Cenozoic marine sediments (Figure 2) were named the Kashi Group and dated primarily by integrated biostratigraphy [e.g., *Tang et al*., 1989; *Zhou*, 2001; *Bosboom et al*., 2011, 2014b]. The overlying continental sediments are characterized by brown clastic sediments with coarsening trend up the section. This is generally interpreted as a fluvial delta plain with a transition to a debris-flow fan facies. The sediments are loosely constrained to the Neogene-Quaternary and show a high degree of diachroneity. It is broadly accepted that the marine-continental transition occurred within the Baxbulak Formation, the uppermost unit within the Kashi Group. The Formation (also spelled Bashibulake Formation) gradually shifts from delta front facies at the piedmont of the Pamir to a sabkha/lacustrine facies in the Tarim basin, characterized by lateritic sandstones interbedded with brown mudstones and brown mudstones interbedded with gypseous sandstones, respectively [e.g., *Tang et al*., 1989; *Ma and Yang*, 2003]. Due to tectonic overprints, a hiatus in the upper part of the Formation is widely recognizable in most sites from the southwestern Tarim Basin [e.g., *Tang et al*., 1992; *Sobel and Dumitru*, 1997; *Cai*, 1999], while the sections with a relatively complete Baxbulak Formation are only distributed along the PTCZ where it was the regional depocenter during the latest Paleogene-early Neogene [*Hao et al*., 2002].

Our study section (39.80°N, 74.75°E, Figure 1c) is the holostratotype of the Baxbulak Formation and holds the greatest potential of preserving a complete Baxbulak Formation [e.g., *CGXRSC*, 1981; *Hao et al*., 1982; *Zhou*, 2001; *Wang and Chen*, 2005]. On the north of the MPT, the Baxbulak section exposes the Kashi Group, including the Baxbulak Formation, and the overlying Keziluoy Formation along a tributary of the Kizilsu River. The transition from marine gypsum deposits to the terrestrial red-beds can be easily recognized at the base of the Baxbulak Formation (Figures 1c and 2a). At our study section, the uppermost marine deposits, the Ulagon Formation, consists of thick beds of greenish mudstone and gypsum, which conformably underlays the Baxbulak Formation. The Baxbulak Formation (Figures 2b and 2c) is characterized by lateritic mudstones intercalated by siltstones, fine-grained, and thin-beds of gypsum. The Keziluoy Formation nearly conformably, if not conformably, overlies the Baxbulak Formation and contains brownish red mudstone, siltstones, and sandstones (Figures 2d and 2e).

3. Sampling and Methods

We set the zero level for sampling to the base of the Baxbulak Formation and collected two or more separate oriented drill cores from each horizon at an interval typically 2–3 m using a portal water-cooled gasoline-powered drill. For the study section, the exposed 740 m terrestrial sequence yielded 867 oriented samples from 414 horizons.

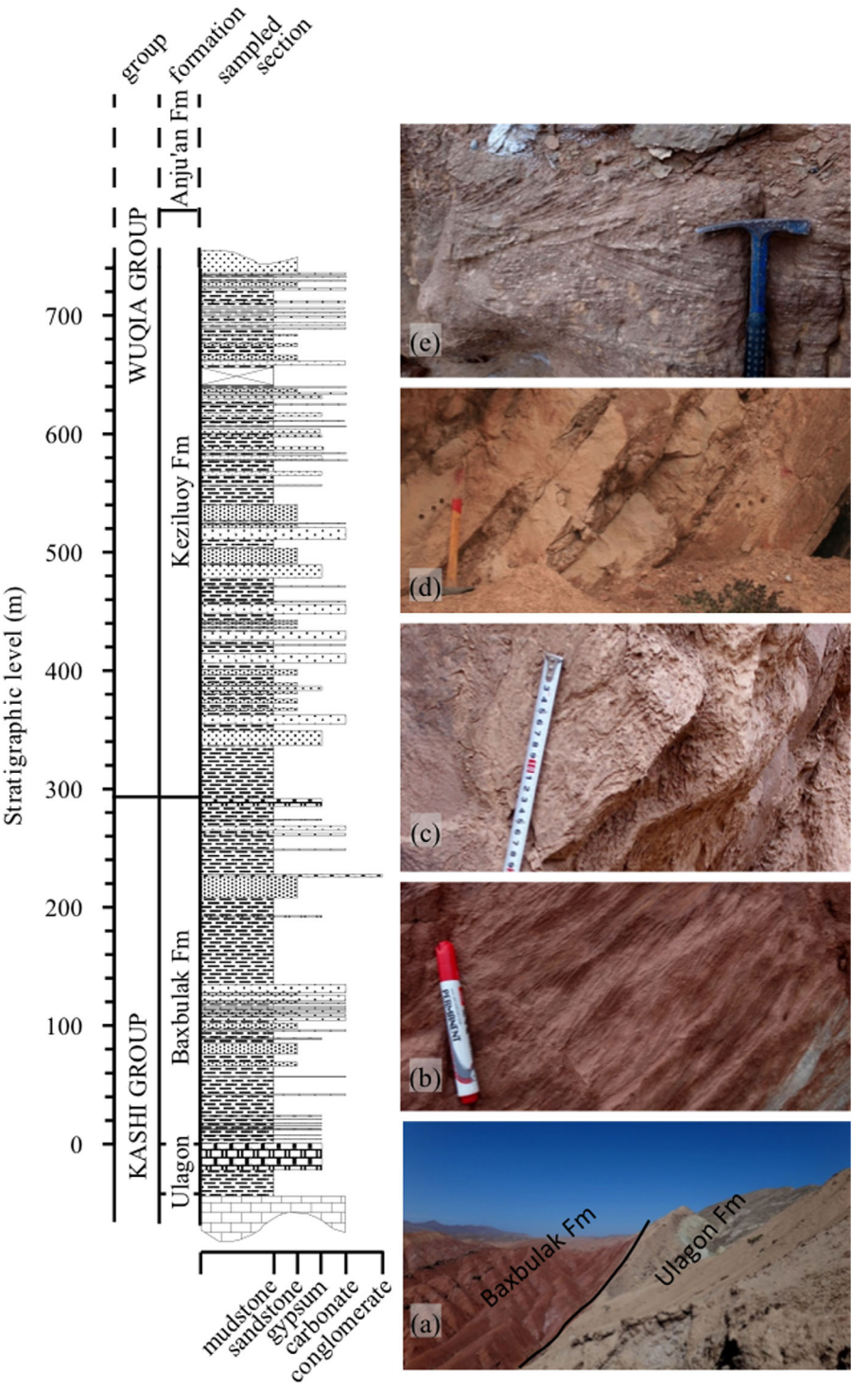

Figure 2. Regional stratigraphic units and lithologic column of the study section. Photos showing sedimentologic features at the Baxbulak section. (a) the marine/terrestrial boundary at the section; (b) ripples in siltstone beds of the upper Baxbulak Formation; (c) tabular cross-bedded sandstone in the upper Baxbulak Formation; (d) couplets of brownish siltstones and mudstones in the lower Keziluoy Formation; and (e) trough cross-bedded siltstone in the middle Keziluoy Formation.

Core samples about 2 cm in length for thermal demagnetization were cut in the laboratory and selected leftovers of these samples were subjected to rock magnetism analysis. The measurements of rock magnetism and paleomagnetism were performed at the Paleomagnetism and Geochronology Laboratory of the Institute of Geology and Geophysics, Chinese Academy of Sciences (IGGCAS). On six selected samples for

different horizons of the section, both temperature independence of magnetic susceptibility (*k*-T curve) and acquisition and backfield demagnetization of isothermal remanent magnetization (IRM) were conducted. The *k*-T curves were measured in a magnetic field of 300 A/m at a frequency of 875 Hz by heating from room temperature to ~700°C in an argon atmosphere, using an AGICO KLY-4 Kappabridge coupled with a CS-3 apparatus. IRM curves and hysteresis loops were determined by a vibrating sample magnetometer (Princeton Measurements, MicroMag 3900) at room temperature. Anisotropy of magnetic susceptibility (AMS) was measured on one oriented specimen for each sampled horizon using an AGICO KLY-3 Kappabridge. It is well documented that tectonic fabrics can be rapidly locked in weakly deformed mudrocks shortly after deposition and prior to lithification [*Borradaile and Henry*, 1997; *Parés*, 2004]. In the Lake Issyk-Kul, merely 300 km NE away from the study section, the directly dated sediments that recorded tectonic fabrics provided the first straightforward estimation of the ~1 kyr lag between sediment deposition and tectonic overprinting [*Larrasoaña et al*., 2011] and revealed an rapid, effective locking (less than 1 m).

Stepwise thermal demagnetization of natural remanent magnetization (NRM) was conducted using an ASC TD-48 thermal demagnetizer. Generally samples were stepwise heated in temperature increments of 50°C–500°C and subsequently by 30 or 15°C to a maximum temperature of 685°C. Magnetizations were measured by a 2G Enterprises 760 three-axis cryogenic magnetometer housed in a magnetically shielded space (<300 nT). Demagnetization results were evaluated on stereographic projections and orthogonal vector component diagrams [*Zijderveld*, 1967]. Principal component directions were calculated using a least squares fitting technique [*Kirschvink*, 1980] and interval mean results evaluated using Watson bipolar mean [*Fisher et al*., 1987]. All the evaluations are conducted using the program PMGSC developed by Randy Enkin.

4. Results

4.1. Rock Magnetism

k-T curves and acquisition and backfield demagnetization of IRM are useful for revealing magnetic mineralogy. The *k*-T curves of the all selected samples from the Baxbulak section feature a major decrease in magnetic susceptibility when heated to around 580°C, with a minor decrease above 600°C (Figure 3a), indicating the presence of magnetite and probably hematite. Most samples show significant increase in magnetic susceptibility at 400–580°C (e.g., samples KZ14, KZ168, BS3, BS41 in Figure 3a), implying that there exists newly formed magnetite. This probably results from dewatered Fe-bearing clay minerals or the thermal breakdown of greigite [*Dunlop and Özdemir*, 2001; *Roberts et al*., 2011], which is present as a rare accessory mineral in some samples.

The presence of mixed magnetite and hematite assemblages is also expressed in IRM acquisition curves and hysteresis loops. Additionally, samples from the Keziluoy Formation showed lower concentrations of hematite than those from the Baxbulak Formation. Specimens from both formations contain a mixture of high and low coercivity minerals, resulting in waspwaisted hysteresis loops that do not reach true saturation even after exposure to applied fields of 1.5 T (Figure 3c). These two coercivity components can be isolated using the method of *Kruiver et al*. [2001] (data provided in supporting information Table S1). However, the greater extent of high coercivity minerals in the Baxbulak Formation samples is also supported by a number of more straightforward observations. First, Baxbulak specimens have higher bulk coercivities and coercivities of remanence (Figure 3b). Second, Baxbulak specimens acquire 80% of the SIRM intensity only after exposure to fields of >600 mT, while Keziluoy specimens are able to acquire this same fraction of SIRM intensity after exposure to a 400 mT applied field. Third, Baxbulak specimens have higher squareness values (Mr/Ms) than those of the Keziluoy Formation. Thermal demagnetization experiments also show significant fractions of remanence persisting between temperatures of 600 and 685°C (Figure 4), indicating that this high coercivity phase is indeed hematite.

4.2. Magnetic Remanence Directions

Stepwise thermal demagnetization trajectories (Figure 4) clearly show that the NRM in most samples is composed of two components: a low-temperature component isolated by the first few steps (generally below 400°C) followed by a characteristic remanent magnetization component (ChRM) isolated at higher temperatures. The ChRM is of dual polarity and decays univectorally toward the origin on orthogonal diagrams. The ChRM is mostly removed at temperature steps between 400 and 685°C, showing a similar magnetization

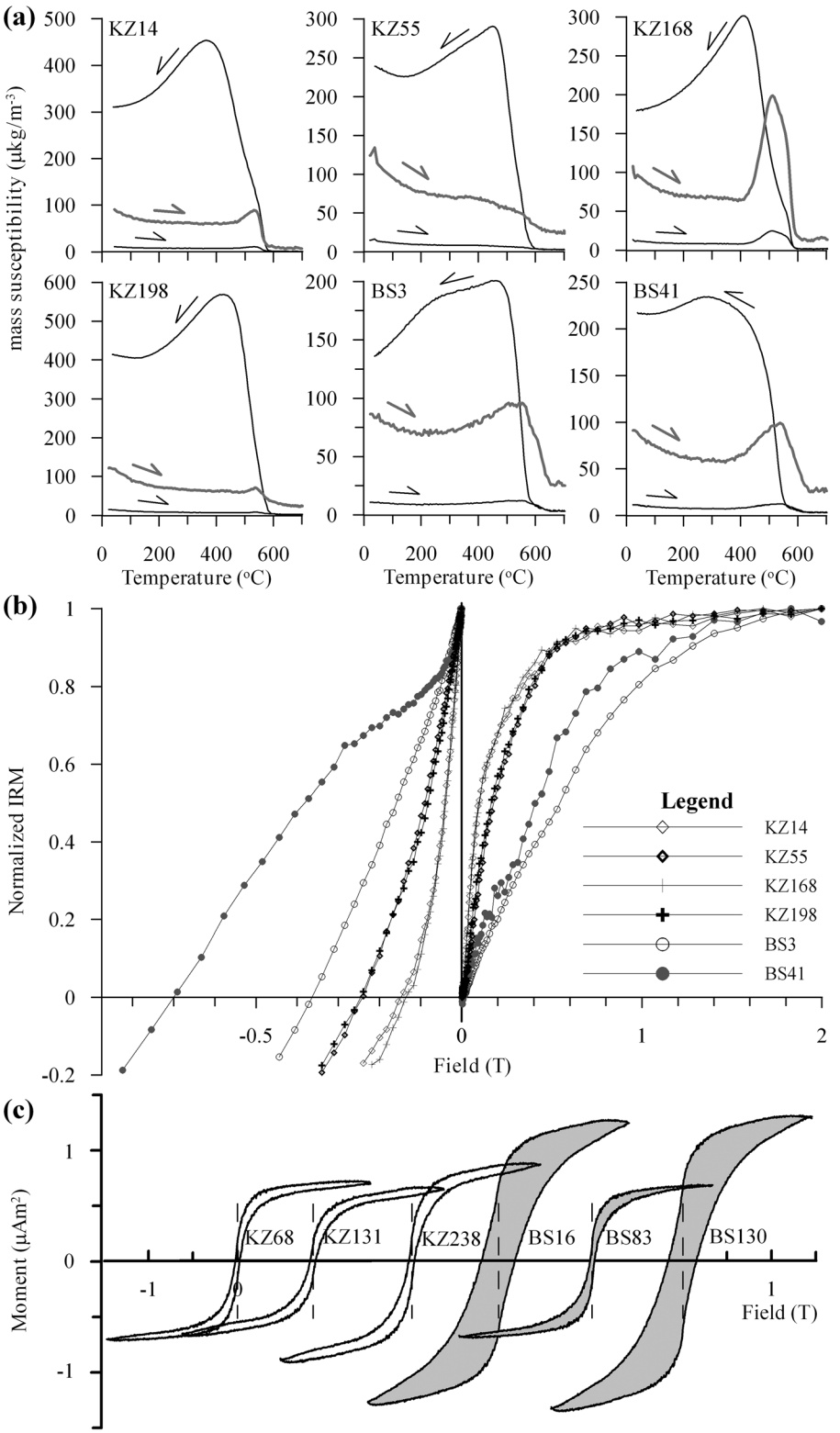

Figure 3. (a) Low-field temperature dependence of magnetic susceptibility (*k*-T curves) of selected samples. The gray thick curve is a eight-fold amplified heating curve just for better display; (b) behavior of acquisition and back-field demagnetization of IRM for the samples. Note the change in the horizontal scale on either side of B = 0; and (c) magnetic hysteresis loops for the samples from the Baxbulak (gray-filled) and Keziluoy Formations.

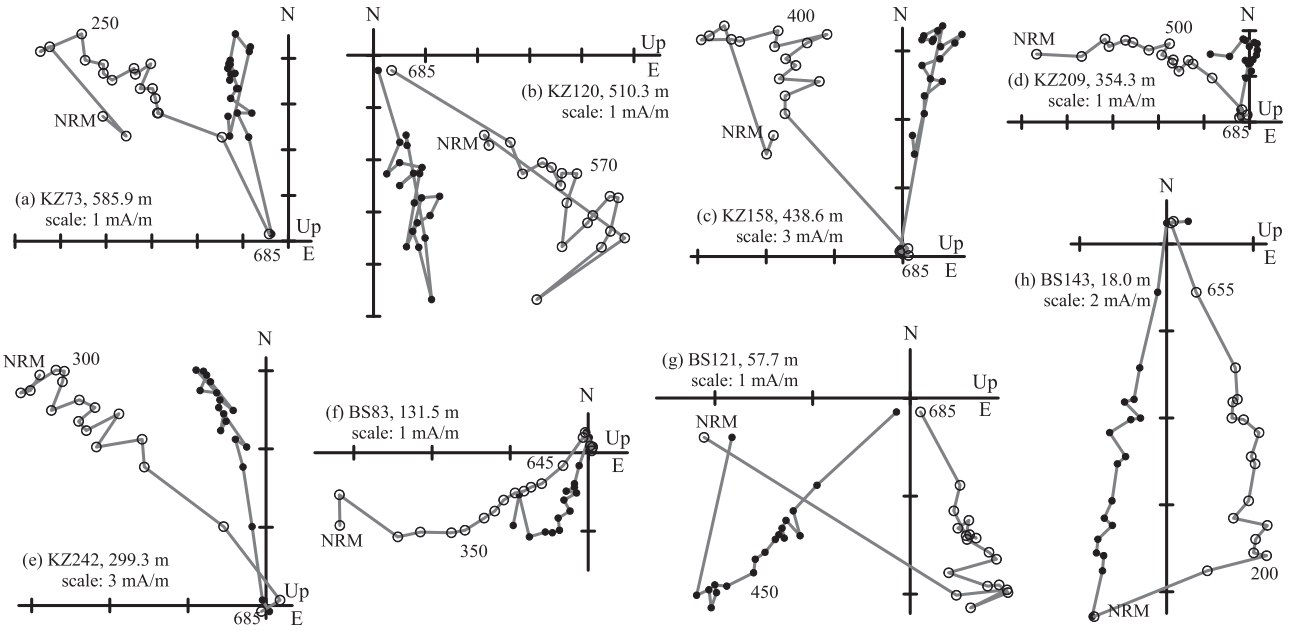

Figure 4. Orthogonal demagnetization diagrams showing typical thermal demagnetization behaviors of the studied samples. Demagnetization steps are in °C, and stratigraphic directions are plotted. Solid and open circles represent vector endpoints projected onto the horizontal and vertical planes, respectively.

direction above and below 580°C. The demagnetization characteristics indicate that hematite and magnetite are the dominant carriers of the ChRM, both recording the similar magnetic field direction.

Following demagnetization, 88 samples out of the 414 samples were rejected because their maximum angular deviations were >15°. The remaining 326 samples yield well-defined ChRMs. After tilt correction, these ChRM directions result in an antipodal distribution of 186 normal and 140 reversed orientations on the stereographic projection (Figure 5a). The 186 normal ChRM directions yield an overall mean of declination D=348.3° and inclination I = 42.4° (k = 7.4, α_{95} = 4.1°), and the 140 reversed ChRM directions yield an overall mean D = 174.8° and I = −36.8° (k = 7.1, α_{95} = 4.8°). Although the means of all polarity zones narrowly fail a reversal test ($\gamma = 7.5 > \gamma_c = 6.3$) [*McFadden and McElhinny*, 1990], when the section is subdivided into five segments, their confidence intervals for the normal and reversal antipodes overlap at the 95% level (plots provided in supporting information Figure S1), thereby passing the bootstrap reversal test [*Tauxe*, 1998]. This suggests that these sediments were deposited in an actively deforming environment that may experience progressive rotation with time [*Sanson-Hysell et al*., 2009].

In order to perform a meaningful test, these 326 ChRM directions are stratigraphically grouped into 21 sites (Table 1). The overall group-mean direction is D = 177.8°, I = 17.1° (k = 2.5, α_{95} = 26.1°) before tilt correction and D = 351.9°, I = 40.2° (k = 50.9, α_{95} = 4.5°) after tilt correction, showing a significant improvement by tilt adjustment (Figure 5b). No tilt test can be performed on the single study section due to the monoclinal bedding (Figure 1c). Here we applied the tilt test to several sites from the PTCZ (NAT and EKQ sections in Figure 1b) where the bedding tilts are markedly different (all data for fold tests provided in supporting information Table S3). The direction-correction tilt test [*Enkin*, 2003] yields an optimum clustering at 94.38 ± 3.37% (Figure 5c), and the syntilt Fisher analysis [*Watson and Enkin*, 1993] produces an optimum degree of untilting at 92.7 ± 2.1% (Figure 5d). Again, the ChRM directions did not pass the tilt tests, possibly because of incomplete isolations of pre-/post-tilting components, and/or differences in age of remanence between the sites. Considering the insignificant differences in the overall mean direction at 90.0% unfolding (D = 351.6°, I = 49.9°, α_{95} = 3.5°) from that at 100% unfolding (D = 351.9°, I = 40.2°, α_{95} = 4.5°), we still assume that the ChRM is of a primary origin.

4.3. Magnetostratigraphy

The declination and inclination of ChRM from 326 horizons were used to calculate virtual geomagnetic pole (VGP) latitude. The VGP latitudes were organized into stratigraphic levels to build the magnetic polarity

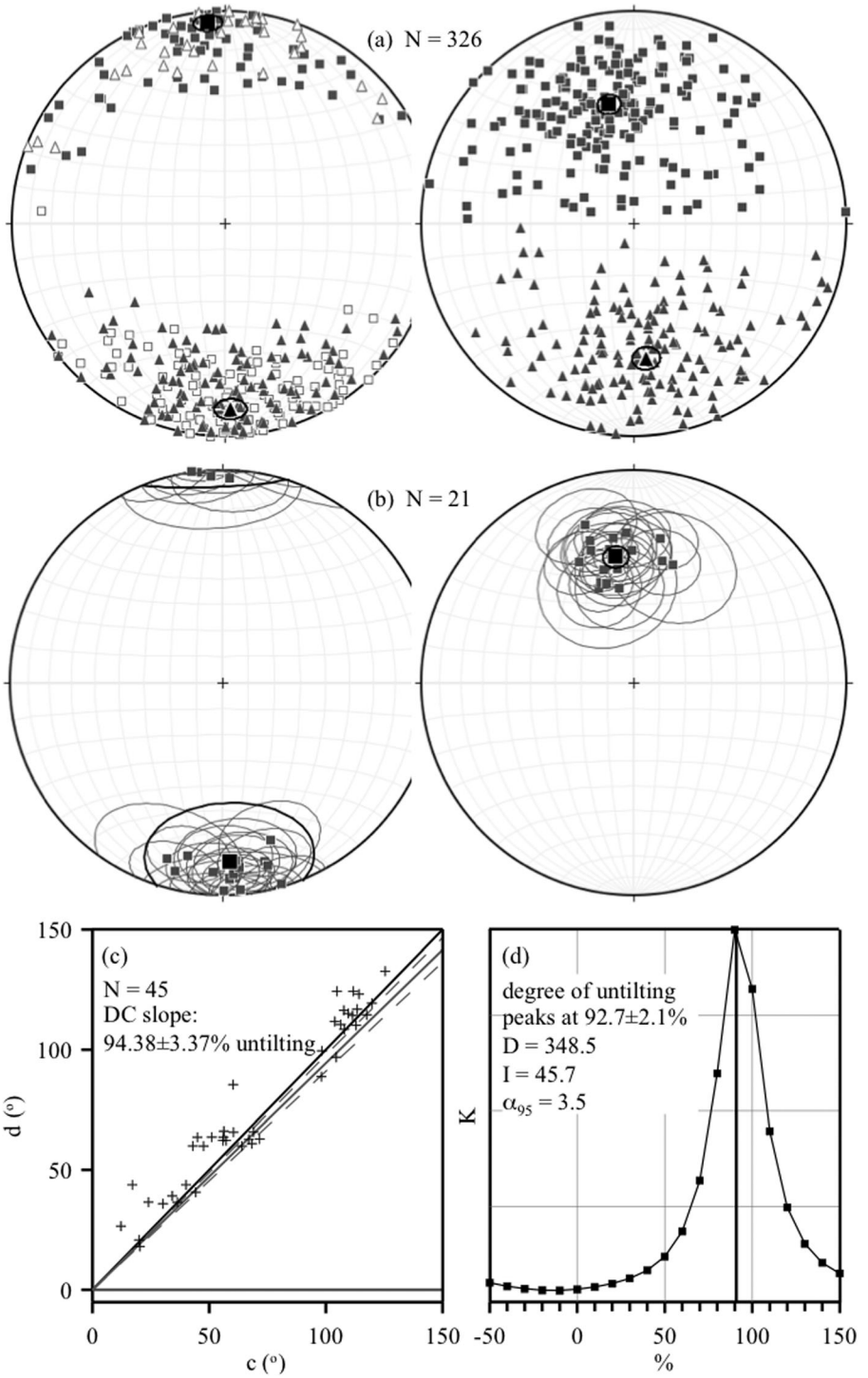

Figure 5. (a) Equal-area stereonet of the 326 ChRM directions at the Baxbulak section, shown in geographic (in situ) and stratigraphic (tilt corrected) coordinates; (b) the stratigraphically grouped 21 sites mean directions (Table 1) of ChRM in geographic and stratigraphic coordinates; (c) the DC tilt test for 45 sites: 21 group-mean directions from the study section, 15 site-mean directions from the EKQ section, and 9 site-mean directions from the NAT section. The sections are marked in Figure 1b; and (d) The syntilt Fisher analysis for the 42 mean directions, showing an optimal degree of untilting at 92.7 ± 2.1%. The required data for fold tests can be found in supporting information files.

sequence, with each chron being constrained by at least two samples from different levels (Figure 6). A total of 13 normal magnetic chrons (N1–N13) and 12 reverse ones were thus identified in the Baxbulak section.

Table 1. Summary of the Interval-Mean Directions of ChRM From the Baxbulak Section

Site ID	Stratigraphic Level (m)	N	Dg	Ig	Ds	Is	ks/kg	$a_{95}s/a_{95}g$
KZ-12	735.4-692.5	15	175.3	16.1	352.1	32.2	5.9/5.9	13.0/13.0
KZ-11	690.7-643.6	17	182.9	12.1	359.4	38.1	5.1/5.1	13.7/13.8
KZ-10	642.1-606.7	14	179.0	18.9	357.2	30.6	5.5/5.5	14.6/14.6
KZ-09	603.5-573.2	15	175.1	2.7	345.4	44.5	10.4/10.4	8.6/8.6
KZ-08	571.0-543.8	17	176.0	9.3	350.0	38.8	8.1/8.1	9.6/9.6
KZ-07	540.0-512.7	13	166.7	15.2	342.8	31.3	6.5/6.5	14.4/14.3
KZ-06	508.4-465.3	15	353.3	0.9	339.9	51.2	4.7/4.7	15.3/15.4
KZ-05	463.4-435.1	14	177.9	8.8	352.4	44.9	6.5/6.6	12.4/12.1
KZ-04	434.0-406.0	19	166.1	12.7	342.2	35.4	8.8/8.8	8.7/8.7
KZ-03	402.5-371.6	15	176.7	11.3	353.1	38.2	6.8/6.8	12.2/12.1
KZ-02	368.9-333.1	18	351.8	0.4	342.0	49.1	6.1/6.3	11.5/11.5
KZ-01	330.7-296.5	18	163.6	2.1	335.9	38.4	5.5/5.5	12.8/12.6
BS-09	291.4-266.1	15	179.5	2.7	351.8	45.3	5.2/5.2	14.9/14.9
BS-08	263.0-239.8	16	194.1	9.6	13.2	41.3	5.2/5.2	13.6/13.6
BS-07	236.7-198.4	17	357.0	3.5	344.8	50.1	3.7/3.7	25.2/25.1
BS-06	197.0-174.2	15	2.1	4.8	351.6	53.2	6.7/6.5	16.0/16.3
BS-05	172.3-140.4	17	191.2	18.7	10.5	32.1	6.0/6.0	12.9/12.9
BS-04	138.6-119.4	14	174.6	14.2	350.0	36.7	5.3/5.2	15.9/16.0
BS-03	117.8-89.9	13	175.7	17.4	352.4	37.2	4.8/4.8	18.8/18.8
BS-02	88.1-44.6	15	197.5	14.8	18.6	41.7	4.1/4.0	22.7/23.0
BS-01	40.9-1.3	14	163.1	23.8	343.1	23.9	5.4/5.4	16.5/16.5
Mean			177.8	17.1	351.9	40.2	50.9/2.5	4.5/26.1

Biostratigraphic information of the underlying and overlying strata constrain a chronological range to the section for magnetostratigraphic correlation. From the greenish mudstone just underlying the gypsum beds at the base of the sampled section, the presence of coccolith *Nannotetrina fulgens* (NP14/NP15 boundary marker) [*Agnini et al*., 2006; *Molina et al*., 2011] indicates its basal age younger than the late Middle Eocene [*Tang et al*., 1989], and the *Ammonia* fauna found in the overlying Anju'an Formation suggests a terminal age older than the mid-Miocene [*Hao et al*., 1982].

With these constraints, we correlated the observed polarity sequence with the geomagnetic polarity time scale (GPTS) [*Ogg*, 2012] using a numerical correlation method based on the Dynamic Time Warping algorithm [*Lallier et al*., 2013]. We ran the program 5000 times to find 50 potential correlation options. As a result, the 10 minimum cost correlations (i.e., best correlating) unanimously date the sequence to the GPTS chrons from C11n.1n to C6An.2n with only a few minor disagreements between them. We adopted the sole option with the least cost (Figure 6), resulting in absolute ages of the section from 29.1 to 20.7 Ma. This preferred correlation also defines the Baxbulak/Keziluoy boundary to be close to the base of the chron C8n.2n, ~26 Ma.

A plot of magnetostratigraphic age versus stratigraphic level (Figure 7) suggests mean sediment accumulation rate (SAR) in the Baxbulak section of 8.4 cm/ka, comparable to those of the surrounding sites from the same period [e.g., *Huang et al*., 2006a,b; *Charreau et al*., 2009a; *Tang et al*., 2012]. Moreover, the plot shows an increase in SAR, from ~8.0 cm/ka to 10.2 cm/ka, occurred at 22.5 Ma, roughly coincident with the appearance of highly frequent sandstones within the study section.

4.4. Anisotropy of Magnetic Susceptibility

Bulk magnetic susceptibility (K_m) and its anisotropy were determined, and corrected anisotropy degree (P_j) and shape parameter (T) were calculated as defined by *Jelinek* [1981], showing significant changes with stratigraphic levels in the study section (Figure 8). K_m ranges from 12.4 to 578.9 μSI with an average of 194.6 ± 96.4 μSI. At 293 m, K_m markedly increases to ~400 μSI from ~133 μSI, followed by a slightly decreasing trend up the section. A similar change is also observed in the P_j sequence that presents a rapid increase at the same stratigraphic level and progressively decreases. However, variations in T remain relatively constant, demonstrating an independent character to the magnitude of anisotropy and magnetic susceptibility of the sample.

Equal-area stereographic projections of the K_{max} and K_{min} principal axes of the AMS ellipsoids are shown in Figure 9. The tilt-corrected K_{max} are grouped in the direction parallel to the fold axis with a low-mean inclination (mean declination = 105.5°, mean inclination = 15.0°), while the tilt-corrected K_{min} show a slight girdle distribution perpendicular to the fold axis. These distribution patterns of the principal axes are also

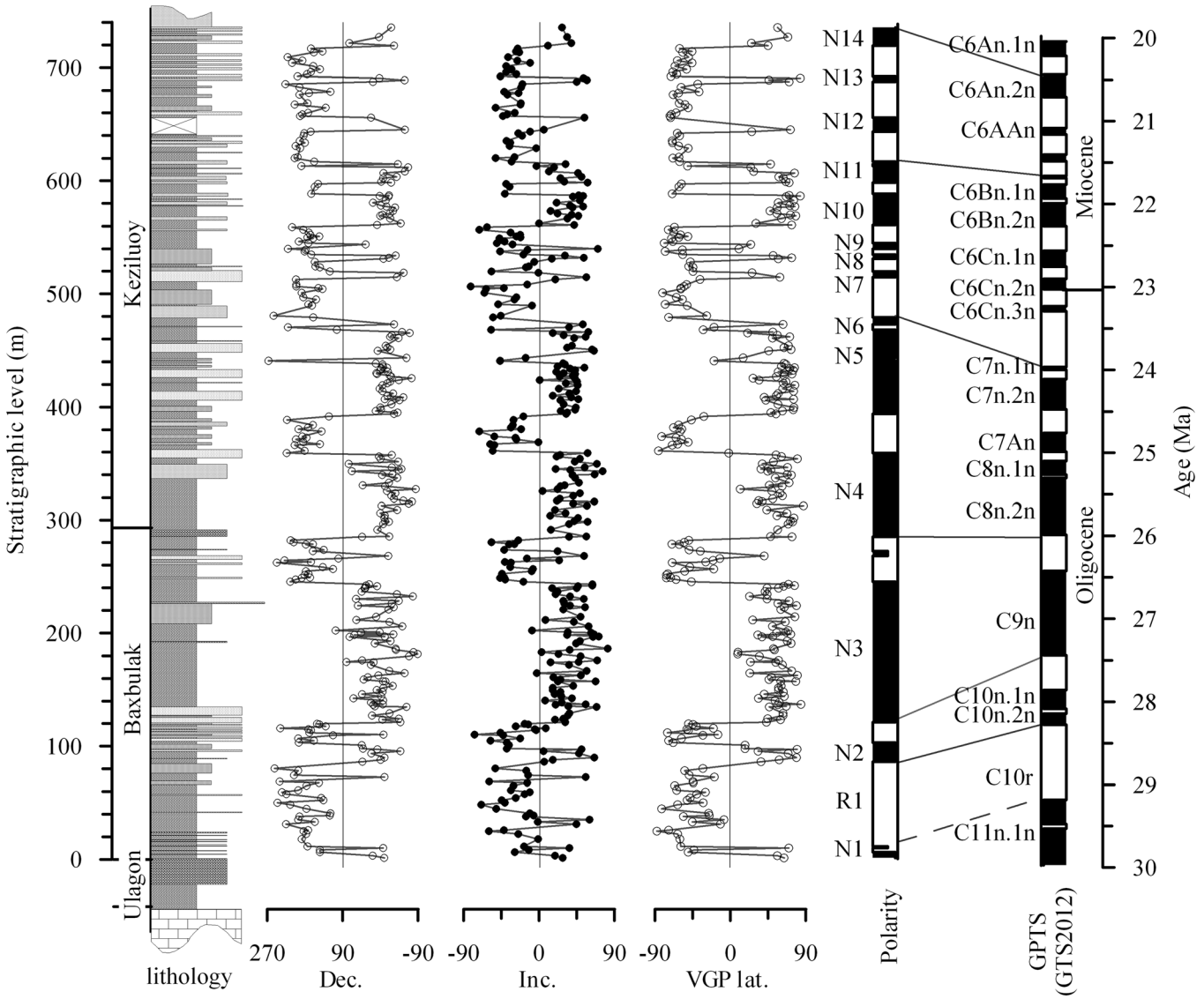

Figure 6. Magnetostratigraphic results of the Baxbulak section and its "least cost" correlation [*Lallier et al.*, 2013] to the GPTS [*Ogg*, 2012].

observed in deformed sediments from neighboring foreland basins [e.g., *Huang et al.*, 2006b; *Charreau et al.*, 2009a; *Tang et al.*, 2012; *Lu et al.*, 2014; *Yu et al.*, 2014].

5. AMS-Derived Tectonic History

Unlike the ChRM behavior, which is dominated by magnetite and hematite (Figure 3), the magnetic properties of the Baxbulak section are largely controlled by only anisotropic hematite. This assertion is based on (1) the overall low K_m (Figure 8), suggesting that the ferromagnetic contribution can be safely neglected and anisotropy is mostly relevant to antiferromagnetic minerals [*Hrouda and Kahan*, 1991]; (2) quantitative estimation of paramagnetic component on the base of thermomagnetic curves (Figure 3a, data provided in supporting information Table S4) [*Hrouda et al.*, 1997]; and (3) the elongated distribution of P_J-T data, both of the Baxbulak and of the Kezluoy Formation, not passing through or toward the magnetite AMS ellipsoid (Figures 10a and 10b) [*Parés*, 2004]. These suggest that the AMS data of the study section expresses a crystallographic preferred orientation for antiferromagnetic minerals, which closely correlated to strain under a variety of sedimentary and tectonic environments [*Borradaile and Henry*, 1997; *Parés*, 2004].

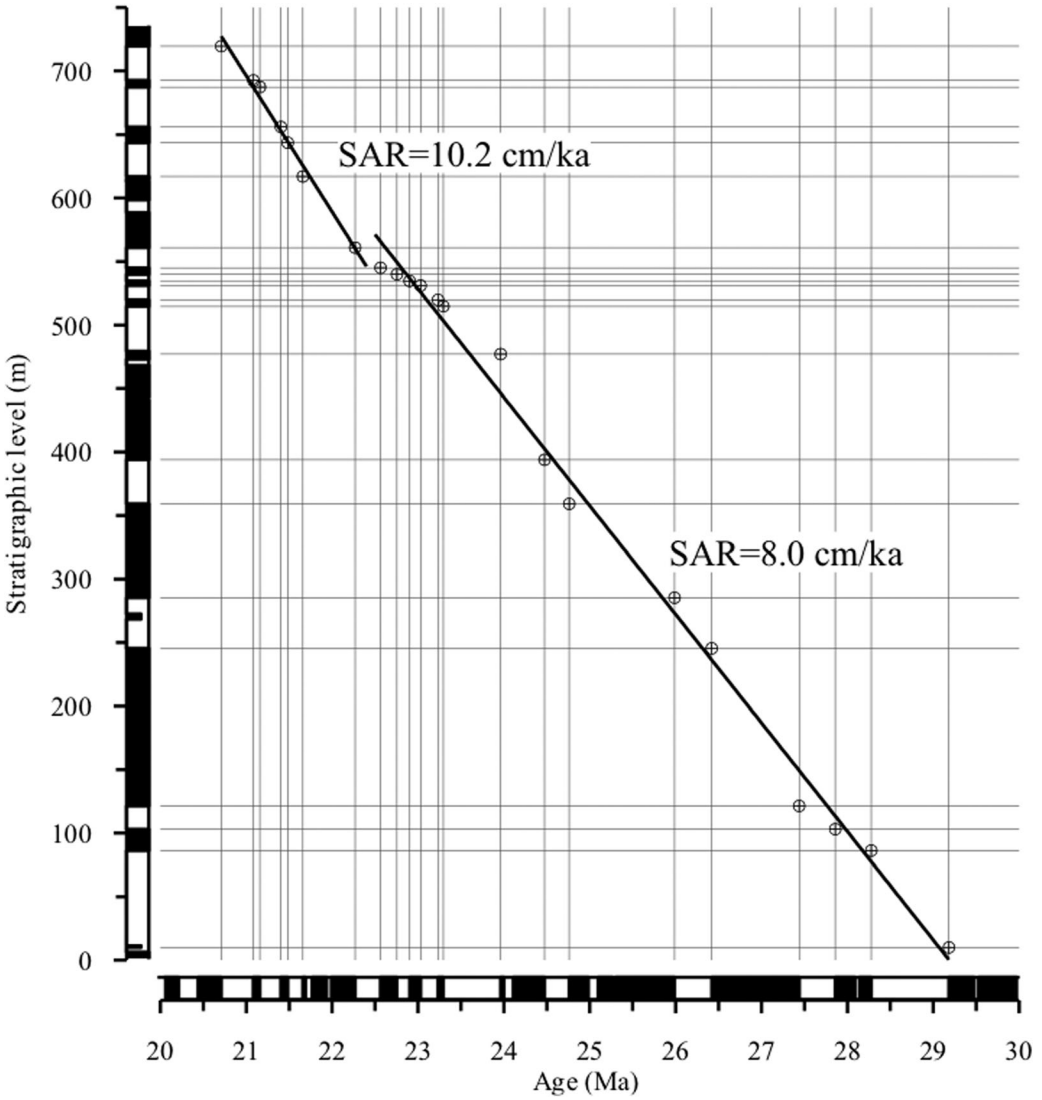

Figure 7. Age versus stratigraphic level plot of the Baxbulak section, using the data from Figure 6.

As observed from neighboring foreland basins, the original magnetic fabric of the study section should survive the competing geological processes, such as sedimentary compaction, transport dynamics, and layer-parallel tectonic strain. Compaction generally results in more oblate fabrics and/or increasing anisotropy degree as a function of depth. Neither is observed from the sequences of T and P_j (Figure 8). If the transport dynamics dominate magnetic fabric signals, one would expect weak anisotropy degrees (commonly below 1.10), mean K_{max} parallel to transportation direction, and mean K_{min} nearly perpendicular to bedding. Specifically, the primary sedimentary fabrics from the study section would be typified by N-S striking K_{max} with K_{min} perpendicular to the bedding, significantly different from the observed fabric records. The observed K_{max} direction of the overall section is near E-W and parallel to the strike of the tilted strata, undoubtedly indicating the overprint of tectonic fabrics to the primary sedimentary fabrics.

In order to track potential changes in the AMS parameters, we divided the section into two parts where the K_m and P_j change and calculated their mean directions of the K_{max} and K_{min} axes (Figure 10). For the lower part of the section, the Baxbulak Formation (Figure 10c, 29.1–26.0 Ma), the K_{min} clustered around the bedding pole with mean inclination of 86.7°, while K_{max} is near parallel to the fold strike, with mean declination of 85.6° and mean inclination of 2.4°, showing a typical character of sedimentary fabric that initially experienced an embryonic overprint by a weak strain [*Borradaile and Henry*, 1997; *Parés*, 2004; *Larrasoaña et al.*, 2011].

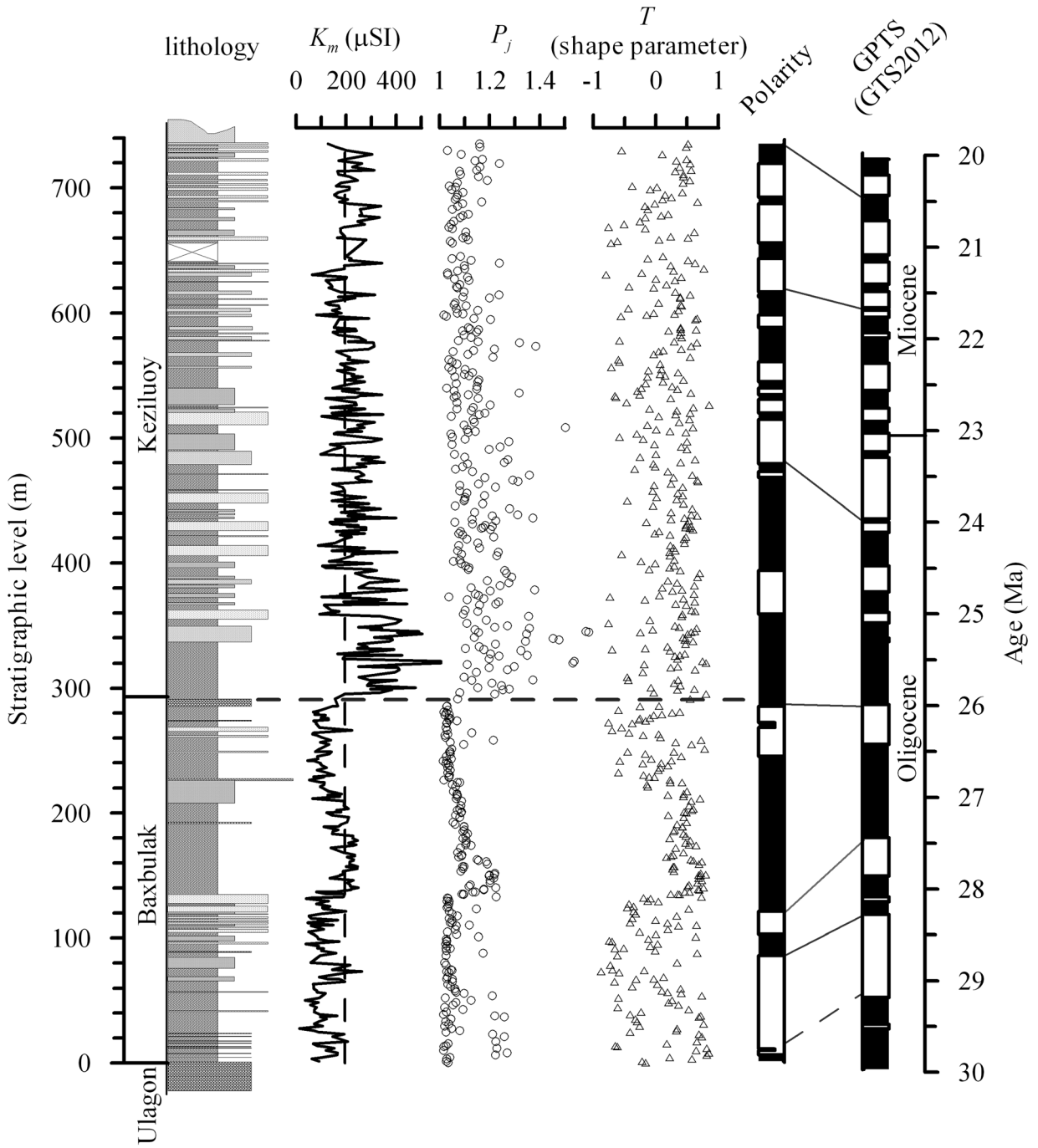

Figure 8. AMS results for the Baxbulak section, showing mean magnetic susceptibility (K_m), corrected AMS degree (P_j), and shape parameter (T). Dashed horizontal line indicates onset of change in susceptibility parameters.

For the upper portion, the Keziluoy Formation (Figure 10d), K_{max} forms a clear girdle distribution roughly along the fold axes (its shape parameter of eigenvalues [*Woodcock*, 1977] is 0.54). Meanwhile, the K_{min} diverts from the bedding pole and is greatly trended to the north, with mean declination of 19.2° and mean inclination of 12.6°, which is along the strain direction. This is a typical feature of tectonic overprint on sedimentary fabric, generally connected with an extensive deformation in strata. Change in the distribution of the principal anisotropy axes suggests that, at least from the basal age of the section, the study region was persistently under a near N-S strain, with a significant increase in strain at 26 Ma.

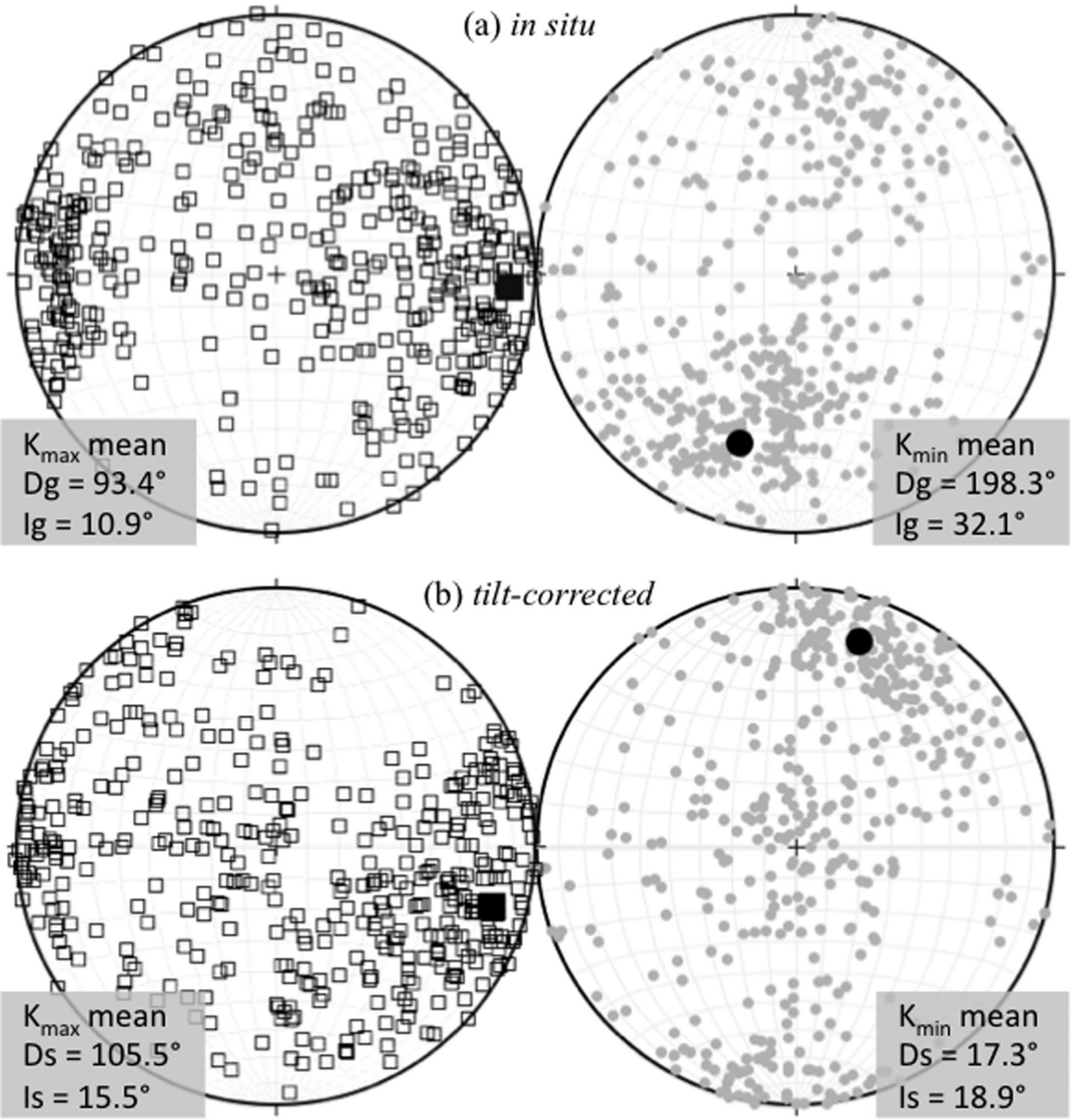

Figure 9. Equal-area stereographic projections of AMS principal axes in geographic (a) and stratigraphic (b) coordinates. Squares and circles denote orientations of K_{max} and K_{min} axes, respectively, and solid squares and circles represent their means.

The increased strain derived from the distributions of principal anisotropy axes is further verified by the increasing anisotropic magnitude (P_j) from the Baxbulak to the Kezluoy Formations, as shown in Figure 8. According to empirical observations [e.g., *Parés and van der Pluijm*, 2002; *Liu and Sun*, 2012; *Tang et al.*, 2012] and numerical simulations [e.g., *Benn*, 1994; *Lehmann et al.*, 2013], the evolution of magnetic parameters P_j and T with strain in mudrocks involves two stages. In the first stage, from compact to weakly deformed regions like foreland basin, the shape of the AMS ellipsoid features a trend from primary oblate ($T > 0$) to prolate ($T < 0$) with increasing strain, while the magnitude of anisotropy (P_j) remains low and stable (i.e., 1.10 or less). The second stage, from foreland basin to shear zone with well-developed tectonite, is characterized by increasing P_j with the AMS ellipsoid returning to oblate. The increase of P_j, together with changes in distribution of K_{max} and K_{min}, clearly suggests that around 26 Ma the PTCZ experienced an increased tectonic strain in nearly N-S direction.

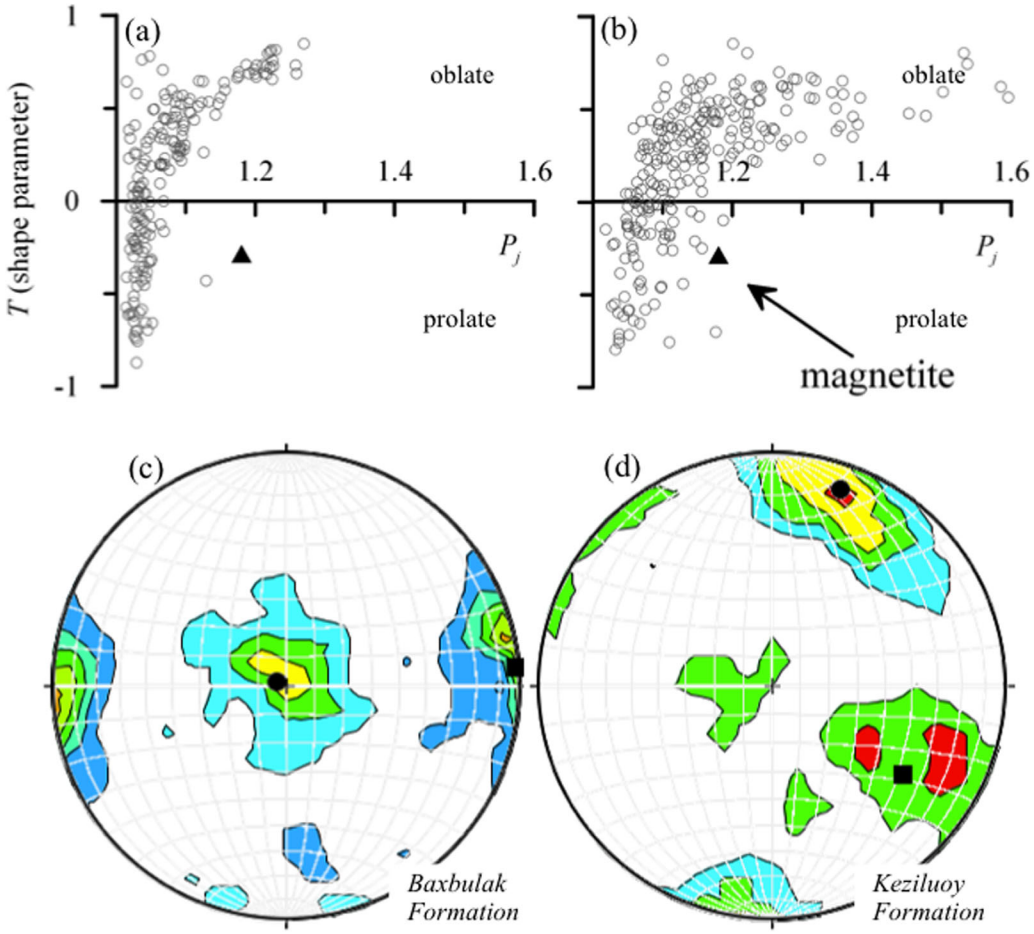

Figure 10. Corrected anistropy degree (P_j) versus shape parameter (T) diagrams and density contour diagrams with contour interval of 2% for AMS data from the Baxbulak section. The data are plotted in two parts to highlight critical changes before (a, c) and after 26 Ma (b, d). Positive (negative) shape parameter values indicate an oblate (prolate) AMS ellipsoid. The AMS ellipsoid for magnetite ($P_j = 1.18$, $T = -0.30$) [*Tarling and Hrouda*, 1993] is shown in subplots a and b by the triangle.

A variety of evidence has strongly demonstrated the late Oligocene tectonic activity around the Pamir. For example, paleomagnetic investigations indicate that counterclockwise vertical-axis rotation of thrust sheets within the Tajik Basin start at the early Miocene [*Thomas et al*., 1994] and that proximal coarse clastic deposition began around the Aertashi region in the southwestern Tarim Basin at ~25 Ma ago [*Yin et al*., 2002]. This suggests that the northward migration of the Pamir initiated at this time. In the Alai Valley, the coarse-grain continental clastic rocks began to be deposited over Mesozoic and early Cenozoic units in the late Oligocene [*Coutand et al*., 2002], reflecting regional tectonic uplift that created the necessary relief and source areas. Moreover, thermochronologic data from central and eastern Pamir [*Sobel and Dumitri*, 1997; *Robinson et al*., 2007; *Amidon and Hynek*, 2010] confirmed this period of accelerated exhumation throughout the region, and further linked this exhumation to initiation of a plate-scale, synchronous crustal thickening [*Amidon and Hynek*, 2010; *Stearns et al*., 2013]. To date, the paleomagnetic data from the PTCZ, as well as available sedimentologic and thermochronlogical data, suggest regional tectonic activity occurred around the late Oligocene.

It is worth noting that the changes in the AMS record reported here seem slightly older than those derived from thermochronologic and sedimentologic evidence, although all of them are related to regional tectonic activities. On the study section, for example, the AMS-inferred strengthening of strain occurred at 26 Ma, ~4 Ma prior to the increase in sedimentary accumulation rate (Figure 7). While this discrepancy could be explained by uncertainties in the dating methods, we highlight the differences in mountain building processes that are recorded by these methods [*Tang et al*., 2012]. The AMS sequence tracks regional strain history that essentially induces crustal deformation, while thermochronologic evidence generally correlates to

Table 2. Review of Paleomagnetic Results From the Surrounding Blocks of the Pamir[a]

		Site					Observed pole			Expected direction			Rotation		
Area	Age	λ_s (°N)	φ_s (°E)	D_o (°)	I_o (°)	α_{95} (°)	λ_{op} (°)	φ_{op} (°)	dp/dm	D_x (°)	I_x (°)	α_{95} (°)	R (°)	ΔR (°)	Source
Western Pamir															
Pulkhakim	Miocene	38.0	67.4	343.6	38.1	17.0	69.0	277.6	8.0/15.0	7.9	57.6	4.2	−24.3	8.0	*Thomas et al.* [1994]
Pyryagata	Miocene	37.7	68.1	338.4	36.7	22.5	64.5	301.5	26.3/15.4	10.9	57.8	3.6	−32.5	12.8	*Thomas et al.* [1994]
S. Darvaz	Eo-Miocene	37.8	68.2	312.0	32.0	9.3	43.4	352.8	10.5/5.9	10.9	57.9	3.6	−58.9	10.3	*Thomas et al.* [1994]
Aksu	Miocene	38.1	68.5	347.8	36.6	18.0	69.4	282.7	21.0/12.3	10.9	58.2	3.5	−23.1	10.5	*Thomas et al.* [1994]
N. Pamir	Paleocene	39.0	70.0	329.0	40.0	7.3	59.1	317.5	5.0/9.0	11.2	58.9	3.3	−42.2	5.6	*Bazhenov and Burtman* [1986]
Central and Ne Pamir															
N. Kashi	Pliocene	39.6	76.0	172.3	−39.1	6.5	71.8	279.6	7.8/4.6	4.7	58.4	2.0	−12.4	6.7	*Huang et al.* [2009]
N. Atushi	Pliocene	39.8	76.1	166.9	−45.1	6.9	−72.9	119.7	8.7/5.5	4.8	58.6	2.0	−17.9	7.6	*Huang et al.* [2009]
	Miocene			161.5	−48.0	8.2	71.4	316.5	10.7/7.0	11.1	60.4	3.4	−29.6	10.0	*Huang et al.* [2009]
EKQ	Miocene	39.8	74.6	348.1	42.0	8.1	71.5	290.9	9.9/6.1	11.1	60.5	3.4	−23.0	9.1	*Huang et al.* [2009]
W. Wuqia	Eocene?	39.8	74.7	336.9	47.4	5.7	67.9	321.1	7.4/4.8	11.5	60.5	4.0	−34.6	8.1	*Huang et al.* [2009]
Chitral	Eocene	36.5	72.3	70.5	59.4	2.3	36.1	135.3	3.0/6.0	13.9	55.6	6.0	56.6	7.2	*Klootwijk et al.* [1994]
NE Pamir	Paleocene	39.4	74.0	43.2	41.5	6.3	50.5	174.0	6.0/10.0	11.2	59.8	3.2	32.0	6.5	Bazhenov and Burtman [1986]
Eastern Pamir															
Qimugen	Miocene	38.5	76.5	3.8	38.0	6.9	72.6	244.5	8.2/4.8	7.4	58.7	2.5	*−3.6*	*7.1*	*Li et al.* [2013]
	Eocene			15.2	30.0	5.6	64.0	221.4	6.2/3.4	14.4	58.2	5.8	*0.8*	*8.4*	*Li et al.* [2013]
Aertashi	<33–24 Ma	38.1	76.4	17.6	36.9	5.0	66.8	210.5	5.9/3.4	9.8	54.7	4.5	7.8	6.3	*Rumelhart et al.* [1999]
	33–27 Ma	38.0	76.6	26.3	37.2	5.8	61.5	196.3	6.8/4.0	9.8	54.6	4.5	16.5	7.2	*Bosboom et al.* [2014a, 2014b]
	41–36 Ma			31.2	28.3	3.4	54.2	197.9	3.7/2.0	14.3	57.7	5.8	16.9	7.4	*Bosboom et al.* [2014a, 2014b]
Kezi	41–40 Ma	38.4	76.4	23.9	36.9	11.1	62.8	200.4	13.0/7.6	14.3	58.1	5.8	13.0	12.3	*Bosboom et al.* [2014a, 2014b]
Puska	Eocene	37.1	78.4	4.3	24.3	8.4	65.3	268.5	9.0/4.8	10.8	58.4	3.3	*−6.5*	*7.9*	*Rumelhart et al.* [2002]

[a]The central Pamir Plateau is bounded by the Darvaz fault to the west and by the KYTS to the east; λ and φ represent latitude and longitude, respectively; D, I, and a95 represent declination, inclination, and associated 95% confidence limits of direction, respectively; Relative rotation to Eurasia [*Besse and Courtillot*, 2002] is recalculated in the direction-space approach following *Butler* [1998] and taken as positive when clockwise; The relative rotation in italics is not statistically distinguishable from the expected direction ($R < \Delta R$).

rapid exhumation of uplifted mountains. In contrast, increasing grain size and accumulation rate in sedimentary basins commonly record enhanced erosional yields and sediment transport capacity, both of which are potentially associated with tectonic uplift [*Hooke*, 2000; *Binnie et al.*, 2007]. In the neighboring region, tectonic-driven conglomerates propagated basinward with great diachrony [e.g., *Chen et al.*, 2007; *Charreau et al.*, 2009b; *Huang et al.*, 2010].

As discussed above, the changes in distribution pattern of AMS principal axes would reflect the strengthening of tectonic strain. Moreover, around 26 Ma, the direction of the AMS principal axes also undergoes a significant change (Figure 10). The mean declination of K_{max} shifts from 85.6 ± 5.6° in the Baxbulak Formation (Figure 10c) to 124.1 ± 13.0° in the Keziluoy Formation (Figure 10d). The mean declination of K_{min} shows a rotation with the similar angle, as observed in the declinations of the ChRMs (Table 1; also plotted in supporting information Figure S2). Two possibilities are tentatively presented here to explain this ~30° rotation: a clockwise rotation of tectonic strain or a counterclockwise rotation of the small block in which the study section is located. To further constrain the tectonic significance of the AMS records, we collect Cenozoic paleomagnetic data from the blocks surrounding the Pamir Plateau and, for consistency, recalculate direction and magnitude of the vertical-axis rotations (Table 2) relative to the stable Eurasia [*Besse and Courtillot*, 2002]. Cenozoic paleomagnetic data from eastern flank of the Pamir demonstrate somewhat clockwise rotations throughout the Cenozoic, with weak trends of decreasing magnitudes and increasing uncertainties. On the western flank the data exhibit significant counterclockwise rotations. To the northeastern Pamir, where the study section is situated, significant, stable counterclockwise rotations are observed, at least since the Miocene. Based on the similarities of direction, magnitude, and the timing of the initiation of the rotation, we confidently attribute the change in direction of the principal axes of the AMS ellipsoid around 26 Ma to counterclockwise rotation of local blocks.

Recent investigations on the KYTS arrived at a consensus that its dextral slip initiated in the late Oligocene, although relevant rotations are still not well constrained [e.g., *Cowgill*, 2010; *Li et al.*, 2013; *Bosboom et al.*, 2014a, 2014b]. To date, the existing data are insufficient to fully understand the kinematic models for the origin of the Pamir indentor, which require further paleomagnetic investigation, as well as study of the structural geology, in the regions near the PTCZ and the KYTS.

6. Concluding Remarks

Our paleomagnetic study shows that the Baxbulak section spans the interval 29.1–20.7 Ma. This result not only indicates that the region between the Pamir and Tian Shan received terrestrial deposits since at least as early as the late Oligocene, but also provides the first temporal constraints for late Oligocene-early Miocene tectonic activity.

The distribution pattern of the AMS principal axes from the section demonstrates that the region was continuously under strain in a N-S direction during the interval and that the strain significantly increased since around 26 Ma, roughly consistent with previous investigations of paleomagnetism, sedimentological analysis, and thermochronology on the Pamir and neighboring regions. Meanwhile, the direction of the AMS principal axes shows a significant counterclockwise rotation, probably associated with tectonic rotations on the local scale.

Acknowledgments

This work was financed by the Chinese Academy of Sciences Key Project (grant XDB03020503), the National Basic Research Program of China (grant 2013CB956404), and the NSFC (grants 41102109, 41472151). We thank Prof. Huang Baochun at Peking University and Prof. Wan Xiaoqiao at China University of Geosciences (Beijing) for insightful discussion, Xu Lishuai, Xi Dangpeng, Jiang Tian, Luo Pan, and Ji Junliang for assistances with fieldwork, and Daniel Hill for reviewing the manuscript. We are also indebted to Joshua Feinberg and an anonymous reviewer, whose constructive comments greatly improved this paper. Supporting data are included as two tables and one figure in the supporting information files. Data for producing Figures 6, 8, and 9 are available from the corresponding author via email.

References

Agnini, C., G. Muttoni, D. V. Kent, and D. Rio (2006), Eocene biostratigraphy and magnetic stratigraphy from Possagno, Italy: The calcareous nannofossil response to climate variability, *Earth Planet. Sci. Lett.*, *241*, 815–830.

Amidon, W. H., and S. A. Hynek (2010), Exhumational history of the north central Pamir, *Tectonics*, *29*, TC5017, doi:10.1029/2009TC002589

Bazhenov, M. L., and V. S. Burtman (1986), Tectonics and paleomagnetism of structural arcs of the Pamir-Punjab syntaxis, *J. Geodyn.*, *5*, 383–396, doi:10.1016/0264-3707(86)90017-7.

Benn, K (1994), Overprinting of magnetic fabrics in granites by small strains: Numerical modelling, *Tectonophysics*, *233*, 153–162, doi: 10.1016/0040-1951(94)90238-0.

Besse, J., and V. Courtillot (2002), Apparent and true polar wander and the geometry of the geomagnetic field over the last 200 Myr, *J. Geophys. Res.*, *107*(B11), 2300, doi:10.1029/2000JB000050.

Binnie, S. A., W. M. Phillips, M. A. Summerfield, and L. K. Fifield (2007), Tectonic uplift, threshold hillslops, and denudation rates in a developing mountain range, *Geology*, *35*, 743–746, doi:10.1130/G23641A.1.

Borradaile, G. J., and B. Henry (1997), Tectonic applications of magnetic susceptibility and its anisotropy, *Earth Sci. Rev.*, *42*, 49–93, doi: 10.1016/S0012-8252(96)00044-X.

Bosboom, R. et al. (2014a), Timing, cause and impact of the late Eocene stepwise sea retreat from the Tarim Basin (west China), *Palaeogeogr. Palaeoclimatol. Palaeoecol.*, *403*, 101–118, doi:10.1016/j.palaeo.2014.03.035.

Bosboom, R., G. Dupont-Nivet, W. Huang, W. Yang, and Z. Guo (2014b), Oligocene clockwise rotations along the eastern Pamir: Tectonic and paleogeographic implications, *Tectonics*, *33*, 53–66, doi:10.1002/2013TC003388.

Bosboom, R. E., et al. (2011), Late Eocene sea retreat from the Tarim Basin (west China) and concomitant Asian paleoenvironmental change, *Palaeogeogr. Palaeoclimatol. Palaeoecol.*, *299*, 385–398, doi:10.1016/j.palaeo.2010.11.019.

Burtman, V. S (2000), Cenozoic srustal shortening between the Pamir and Tien Shan and a reconstruction of the Pamir-Tien Shan transition zone for the Cretaceous and Palaeogene, *Tectonophysics*, *319*, 69–92, doi:10.1016/S0040-1951(00)00022-6.

Burtman, V. S., and P.H. Molnar (1993), Geological and geophysical evidence for deep subduction of continental crust beneath the Pamir, *Geol. Soc. Am. Spec. Pap.*, *281*, 1–76.

Butler, R. F. (1998), *Paleomagnetism: Magnetic domains to Geologic Terranes* [electronic], 23 pp., Blackwell Sci. Publ., Boston.

Cai, T. (1999), *Lithostratigraphy of Xinjiang Uygur Autonomous Region*, pp. 1–430, China Univ. of Geosci. Press, Wuhan.

CGXSC (Compiling Group for Xinjiang Regional Stratigraphic Chart) (1981), *Regional Stratigraphic Scale of Northwest China: Volumn on Xinjiang Uygur Autonomous Region*, Geol. Press, Beijing.

Charreau, J., et al. (2009a), Neogene uplift of the Tianshan mountains observed in the magnetic record of the Jingou River section (Northwest China), *Tectonics*, *28*, TC2008, doi:10.1029/2007TC002137.

Charreau, J., C. Gumiaux, J.-P. Avouac, R. Augier, Y. Chen, L. Barrier, S. Gilder, S. Dominguez, N. Charles, and Q. Wang (2009b), The Neogene Xiyu Formation, a diachronous prograding gravel wedge at front of the Tianshan: Climatic and tectonic implications, *Earth. Planet. Sci. Lett.*, *287*, 298–310, doi:10.1016/j.epsl.2009.07.035.

Chen, J., R. Heermance, D. W. Burbank, K. M. Scharer, J. Miao, and C. Wang (2007), Quantification of growth and lateral propagation of the Kashi anticline, southwest Chinese Tian Shan, *J. Geophys. Res. 112*, B03S16, doi:10.1029/2006JB004345.

Chen, Y., J. P. Cogné, and V. Courtillot (1992), New Cretaceous paleomagnetic poles for the Tarim Basin, Northwestern China, *Earth Planet. Sci. Lett.*, *114*, 17–38.

Coutand, I., M. R. Strecker, J. R. Arrowsmith, G. Hilley, R. C. Thiede, A. Korjenkov, and M. Omuraliev (2002), Late Cenozoic tectonic development of the intramontane Alai Valley, (Pamir-Tien Shan region, central Asia): An example of intracontinental deformation due to the Indo-Eurasia collision, *Tectonics*, *21*(6), 1053, doi:10.1029/2002TC001358.

Cowgill, E. (2010), Cenozoic right-slip faulting along the eastern margin of the Pamir salient, northwestern China, *Geol. Soc. Am. Bull.*, *122*, 145–161, doi:10.1130/B26520.1.

Dunlop, D.J., and Ö. Özdemir (2001), *Rock Magnetism: Fundamentals and Frontiers*, Cambridge Univ. Press, Cambridge, U. K.

Dupont-Nivet, G., Z. Guo, R. F. Butler, and C. Jia (2002), Discordant paleomagnetic direction in Miocene rocks from the central Tarim Basin: Evidence for local deformation and inclination shallowing, *Earth Planet. Sci. Lett.*, *199*, 473–482.

Enkin, R. J. (2003), The direction–correction tilt test: An all-purpose tilt/fold test for paleomagnetic studies, *Earth Planet. Sci. Lett.*, *212*, 151–166, doi:10.1016/s0012-821x(03)00238-3.

Fisher, N.I., T. Lewis, and B. J. J. Embleton (1987), *Statistical Analysis of Spherical Data*, Cambridge Univ. Press, Cambridge.

Hao, Y., X. Zeng, and H. Li (1982), Late Cretaceous and Tertiary strata and foraminifera in western Tarim Basin [in Chinese with English abstract], *Earth Sci.*, *2*, 1–154.

Hao, Y., S. Guan, L. Ye, Y. Huang, Y. Zhou, and S. Guan (2002), Neogene stratigraphy and palaeogeography in the western Tarim Basin [in Chinese with English abstract], *Acta Geol. Sin.*, *76*, 289–298.

Hooke, R. L. (2000), Toward a uniform theory of clastic sediment yield in fluvial systems, *Geol. Soc. Am. Bull.*, *112*, 1778–1786.

Hrouda, F., and š. Kahan (1991), The magnetic fabric relationship between sedimentary and basement nappes in the High Tatra Mountains, N. Slovakia, *J. Struct. Geol.*, *13*, 431–442, doi:10.1016/0191-8141(91)90016-C.
Hrouda, F., V. Jelínek, and K. Zapletal (1997), Refined technique for susceptilibity resolution into ferromagnetic and paramagnetic components based on susceptibility temperature-variation measurement, *Geophys. J. Int.*, *129*, 715–719.
Huang, B., J. Piper, S. Peng, T. Liu, Z. Li, Q. Wang, and R. Zhu (2006a), Magnetostragraphic study of the Kuche Depression, Tarim Basin, and Cenozoic uplift of the Tian Shan Range, Western China, *Earth. Planet. Sci. Lett.*, *251*, 346–364, doi:10.1016/j.epsl.2006.09.020.
Huang, B., J. Piper, Y. Wang, H. He, and R. Zhu (2006b), Paleomagnetic and geochronological constraints on the post-collisional northward convergence of the southwest Tian Shan, NW China, *Tectonophysics*, *409*, 107–124, doi:10.1029/2005JB003890.
Huang, B., J. D. A. Piper, and R. Zhu (2009), Paleomagnetic constraints on neotectonic deformation in the Kashi depression of the western Tarim Basin, NW China, *Int. J. Earth. Sci.*, *98*, 1469–1488, doi:10.1007/s00531-008-0401-5.
Huang, B., J. D. A. Piper, Q. Qiao, H. Wang, and C. Zhang (2010), Magnetostratigraphic and rock magnetic study of the Neogene upper Yaha section, Kuche Depression (Tarim Basin): Implications to formation of the Xiyu conglomerate formation, NW China, *J. Geophys. Res.*, *115*, B01101, doi:10.1029/2008JB006175.
Jelinek, V. (1981), Characterization of the magnetic fabric of rocks, *Tectonophysics*, *79*, T63–T67, doi:10.1016/0040-1951(81)90110-4.
Kirschvink, J. L. (1980), The least-squares line and plane and the analysisi of palaeomagenetic data, *Geophys. J. R. Astron. Soc.*, *62*, 699–718.
Klootwijk, C. T., P. J. Conaghan, R. Nazirullah, and K. A. de Jong (1994), Further palaeomagnetic data from Chitral (Eastern Hindukush): Evidence for an early India-Asia contact, *Tectonophysics*, *237*, 1–25, doi:10.1016/0040-1951(94)90156-2.
Kruiver, P.P., M. J. Dekkers, and D. Heslop (2001), Quantification of magnetic coercivity components by the analysis of acquisition curves of isothermal remanent magnetisation, *Earth Planet. Sci. Lett.*, *189*, 269–276, doi:10.1016/S0012-821X(01)00367-3.
Lallier, F., C. Antonie, J. Charreau, G. Gaumon, and J. Ruiu (2013), Management of ambiguities in magnetostratigraphy correlation, *Earth Planet. Sci. Lett.*, *371–372*, 26–36, doi:10.1016/j.epsl.2013.04.019.
Larrasoaña, J. C., M. Gómez-Paccard, S. Giralt, and A. P. Roberts (2011), Rapid locking of tectonic magnetic fabrics in weakly deformed mudrocks, *Tectonophysics*, *507*, 16–25, doi:10.1016/j.tecto.2011.05.003.
Lehmann, J., K. Schulmann, J.-B. Edel, J. Ježek, F. Hrounda, O. Lexa, and F. Chopin (2013), Structral and anisotropy of magnetic susceptibility records of granitoid sheets emplacement during growth of a continental gneiss dome (Central Sudetes, European Variscan Belt), *Tectonics*, *32*, 797–820, doi:10.1002/tect.20028.
Li, Z., L. Ding, P. C. Lippert, and H. Wei (2013), Paleomagnetic constraints on the Cenozoic kinematic evolution of the Pamir plateau from the Western Kunlun Shan foreland, *Tectonophysics*, *603*, 257–271, doi:10.1016/j.tecto.2013.05.040.
Liu, W., and J. Sun (2012), High-resolution anisotropy of magnetic susceptibility record in the central Chinese Loess Plateau and its paleoenvironment implications, *Sci. China Earth Sci.*, *55*, 488–494, doi:10.1007/s11430-011-4354-3.
Lu, H., E. Wang, and K. Meng (2014), Paleomagnetism and anisotropy of magnetic susceptibility of the Tertiary Janggalsay section (southeast Tarim basin): Implications for Miocene tectonic evolution of the Altyn Tagh Range, *Tectonophysics*, *618*, 67–78, doi:10.1016/j.tecto.2014.01.031.
Ma, H.-d., and Z.-j. Yang (2003), Evolution of the Cenozoic in southwestern Tarim Basin [in Chinese with English abstract], *Xinjiang Geol.*, *21*, 92–95.
McFadden, P., and M. McElhinny (1990), Classification of the reversal test in palaeomagnetism, *Geophys. J. Int.*, *103*, 725–729, doi:10.1111/j.1365-246X.1990.tb05683.x.
Molina, E., L. Alegret, E. Apellaniz, G. Bernaola, F. Caballero, J. Dinarès-Turell, J. Hardenbol, C. Heilmann-Clausen, J. C. Larrasoana, and H. Luterbacher (2011), The Global Stratotype Section and Point (GSSP) for the base of the Lutetian Stage at the Gorrondatxe section, Spain, *Episodes*, *34*, 86–108.
Ogg, J. G (2012), Geomagnetic polarity time scale, in *The Geologic Time Scale 2012*, edited by F. M. Grastein et al., pp. 85–113, Elsevier, Amsterdam.
Parés, J. M. (2004), How deformed are weakly deformed mudrocks? Insights from magnetic anisotropy, in *Magnetic Fabric: Methods and Applications*, edited by F. Martín-Hernández et al., *Geol. Soc. Spec. Publ.*, *238*, pp. 191–203.
Parés, J. M., and B. A. van der Pluijm (2002), Evaluating magnetic lineations (AMS) in deformed rocks, *Tectonophysics*, *350*, 283–298, doi:10.1016/S0040-1951(02)00119-1.
Reigber, C., G. W. Michel, R. Galas, D. Angermann, J. Klotz, J. Y. Chen, A. Papschev, R. Arslanov, V. E. Tzurkov, and M. C. Ishanov (2001), New space geodetic constrains on the distribution of deformation in central Asia, *Earth. Planet. Sci. Lett.*, *191*, 157–165, doi:10.1016/S0012-821X(01)00414-9.
Roberts, A. P., L. Chang, C. J. Rowan, C. S. Horng, and F. Florindo (2011), Magnetic properties of sedimentary greigite (Fe_3S_4): An update, *Rev. Geophys. 49*, RG1002, doi:10.1029/2010RG000336.
Robinson, A. C., A. Yin, C. E. Manning, T. M. Harrison, S.-H. Zhang, and X.-F. Wang (2007), Cenozoic evolution of the eastern Pamir: Implications for strain-accommodation mechanisms at the western end of the Himalayan-Tibetan orogen, *Geol. Soc. Am. Bull. 119*, 882–896, doi:10.1130/B25981.1.
Rumelhart, P. E., A. Yin, E. Cowgill, R. Butler, Q. Zhang, and X.-F. Wang (1999), Cenozoic vertical-axis rotation of the Altyn Tagh fault system, *Geology*, *27*, 819–822.
Sanson-Hysell, N. J., A. C. Maloof, B. P. Weiss, and D. A. D. Evans (2009), No asymmetry in geomagnetic reversals recorded by 1.1-billion-year-old Keweenawan basalts, *Nat. Geosci.*, *2*, 713–717, doi:10.1038/ngeo622.
Şengör, A. M. C. (1984), The cimmeride orogenic system and the tectonics of Eurasia, *Geol. Soc. Am. Spec. Pap.*, *195*, 1–74.
Sobel, E. R., and T. A. Dumitru (1997), Thrusting and exhumation around the margins of the western Tarim basin during the India-Asia collision, *J. Geophys. Res. 102*(B3), 5043–5063, doi:10.1029/96JB03267.
Stearns, M. A., B. R. Hacker, L. Ratschbacher, J. Lee, J. M. Cottle, and A. Kylander-Clark (2013), Synchronous Oligocene–Miocene metamorphism of the Pamir and the north Himalaya driven by plate-scale dynamics, *Geology*, *41*, 1071–1074, doi:10.1130/g34451.1.
Strecker, M. R., W. Frisch, M. W. Hamburger, L. Ratschbacher, S. Semiletkin, A. Zamoruyev, and N. Sturchio (1995), Quaternary deformation in the Eastern Pamirs, Tadzhikistan and Kyrgyzstan, *Tectonics*, *14*(5), 1061–1079, doi:10.1029/95TC00927.
Sun, J., and M. Jiang (2013), Eocene seawater retreat from the southwest Tarim Basin and implications for early Cenozoic tectonic evolution in the Pamir Plateau, *Tectonophysics*, *588*, 27–38, doi:10.1016/j.tecto.2012.11.031.
Tang, T., H. Yang, X. Lan, C. Yu, Y. Xue, Y. Zhang, J. Wei, L. Hu, and S. Zhong (1989), *Marine Late Cretaceous and Early Tertiary Stratigraphy and Petroleum Geology in Western Tarim Basin, China* [in Chinese with English abstracts], pp. 1–155, Sci. Press, Beijing.
Tang, T., Y. Xue, and C. Yu (1992), *Characteristics and Sedimentary Environments of the Late Cretaceous to Early Tertiary Marine Strata in the Western Tarm Basin, China*, [in Chinese with English abstracts], pp. 1–114, Sci. Press, Beijng.

Tang, Z., B. Huang, X. Dong, J. Ji, and Z. Ding (2012), Anisotropy of magnetic susceptibility of the Jingou River section: Implications for late Cenozoic uplift of the Tian Shan, *Geochem. Geophys. Geosyst.*, *13*, Q03022, doi:10.1029/2011GC003966.

Tapponnier, P., and P. Molnar (1979), Active faulting and Cenozoic tectonics of the Tien Shan, Mongolia, and Baykal regions, *J. Geophys. Res.*, *84*(B7), 3425–3459, doi:10.1029/JB084iB07p03425.

Tarling, D. H., and F. Hrouda (1993), *Magnetic Anisotropy of Rocks*, pp. 1–217, Chapman and Hall, London, U. K.

Tauxe, L. (1998), *Paleomagnetic Principles and Practice*, pp. 1–299, Kluwer Acad. Publ., N. Y.

Thomas, J. C., D. Gapais, P. R. Cobbold, V. Meyer, and V. S. Burtman (1994), Tertiary kinematics of the Tadjik depression (central Asia): Inferences from fault and fold patterns, in *Geodynamic Evolution of Sedimentary Basins, International Symposium*, F. Roure et al., pp. 171–180, Moscow.

Wang, X., and X. Chen (2005), *Stratigraphic Division and Correlation of China*, pp. 1–596, Geol. Publ. House, Beijing.

Watson, G. S., and R. J. Enkin (1993), The fold test in paleomagnetism as a parameter estimation problem, *Geophys. Res. Lett.*, *20*(19), 2135–2137, doi:10.1029/93GL01901.

Woodcock, N. H. (1977), Specification of fabric shapes using an eigenvalue method, *Geol. Soc. Am. Bull.*, *88*, 1231–1236, doi:10.1130/0016-7606(1977)88<1231:sofsua>2.0.co;2.

Yin, A., et al. (2002), Tectonic history of the Altyn Tagh fault system in northern Tibet inferred from Cenozoic sedimentation, *Geol. Soc. Am. Bull.*, *114*, 1257–1295, doi:10.1130/0016-7606(2002)114<1257:thotat>2.0.co;2.

Yu, X., S. Fu, S. Guan, B. Huang, F. Cheng, X. Cheng, T. Zhang, and Z. Guo (2014), Paleomagnetism of Eocence and Miocene sediments from the Qaidam basin: Implications for no integral rotation since the Eocene and a rigid Qaidam block, *Geochem. Geophys. Geosyst. 15*, 2109–2127, doi:10.1002/2014GC005230.

Zhou, Z. (2001), *Stratigraphy of the Tarim Basin* [in Chinese with English abstracts], pp. 1–359, Sci. Press, Beijing.

Zijderveld, J. D. A (1967), AC demagnetization of rocks: Analysis of results, *Meth. Palaeomagn.*, *3*, 254–268.

Zubovich, A. Z., et al. (2010), GPS velocity field for the Tien Shan and surrounding regions, *Tectonics*, *29*, TC6014, doi:10.1029/2010TC002772.